COMMUNICATIONS IN COMPUTATIONAL PHYSICS
Vol. **5**, No. 2-4, pp. 413-425

Commun. Comput. Phys.
February 2009

Modes of a Plasma-Filled Waveguide Determined by a Numerical *hp* Method

K. Appert[1,*], M. Azaïez[2] and R. Gruber[3]

[1] *Centre de Recherches en Physique des Plasmas, Ecole Polytechnique Fédérale de Lausanne, 1015 Lausanne, Switzerland.*
[2] *TREFLE, (UMR CNRS 8505), Ecole Nationale Supérieure de Chimie et de Physique de Bordeaux, Pessac, France.*
[3] *Laboratory of Computational Engineering, Ecole Polytechnique Fédérale de Lausanne, 1015 Lausanne, Switzerland.*

Received 28 September 2007; Accepted (in revised version) 8 January 2008

Available online 1 August 2008

Abstract. We present the application of the recent physics-conforming COOL method [2, 4] to the eigenvalue problem of a cylindrical waveguide filled with unmagnetized plasma. Using the Fourier transform only *along* the waveguide and not in poloidal direction, this is a relevant test case for a numerical discretization method in two dimensions (radial and poloidal). Analytically, the frequency spectrum consists of discrete electromagnetic parts and, depending on the electron density profile of the plasma, of infinitely degenerate and/or continuous, essentially electrostatic parts. If the plasma is absent, the latter reduces to the infinitely degenerate zero eigenvalue of electrostatics. A good discretization method for the Maxwell equations must reproduce these properties. It is shown here that the COOL method meets this demand properly and to very high precision.

PACS: 02.60.Lj, 02.70.Hm, 03.50.De, 41.20.Jb

Key words: COOL method, physics-conforming, continuous spectrum, plasma waveguide, spectral method.

1 Introduction

The paper describes the generalization of a finite element approach that has successfully been used in the past to compute the stability behaviour of Tokamaks [9, 10] and Alfvén wave heating [3] of such fusion devices. In these applications the fundamental

*Corresponding author. *Email addresses:* `Kurt.Appert@epfl.ch` (K. Appert), `azaiez@enscpb.fr` (M. Azaïez), `Ralf.Gruber@epfl.ch` (R. Gruber)

numerical problems were the elimination of the so-called spectral pollution arising from standard finite elements and the poor precision of pollution-free conforming finite elements [9]. This mathematically non-conforming numerical approach proposed in [8, 9] not only eliminated spectral pollution but also delivered high precision solutions with superconvergence properties although only polynomials of order $p=1$ and 0 had been used.

Recently, the COOL (Constraints Oriented Library) method [2] has generalized this older approach to higher order polynomial degrees $p>1$. In this hp method (h being a measure of the discretization) each term of the variational form is represented by a polynomial of degree $p-1$ in each direction, and is discontinuous across all element borders. Internal constraints such as $\vec{\nabla}\cdot\vec{B}=0$ or $\vec{\nabla}\times\vec{E}=0$ can then be identically satisfied. This enables reaching lower energy levels, thus, approximating better the underlying physics.

Mathematically, the magnetohydrodynamic (MHD) Alfvén waves have a lot in common with the electrostatic Langmuir oscillations in unmagnetized cold plasma [3]. In a waveguide filled with cold plasma the electromagnetic waveguide modes are, in general, coupled among themselves and to the Langmuir oscillations. The degree of coupling depends on the mode frequency and the density gradient of the plasma. It is therefore impossible to impose explicitly conditions like $\vec{\nabla}\times\vec{E}=0$ for dominantly electrostatic modes or $\vec{\nabla}\cdot\vec{E}=0$ for electromagnetic ones, respectively; some modes may show such a character to a high degree and others not. Their property must be the result of the calculation and cannot be imposed externally. In the limiting case of vanishing plasma density, the frequency of the electrostatic oscillation tends to zero: These eigensolutions correspond to the electrostatic solutions of Maxwell's equations in vacuo. If standard finite elements are used in this case, the infinitely degenerate zero eigenvalues appear as a series of discrete eigenvalues with an accumulation point at zero, an unacceptable result! With standard triangular elements, the number of constraints to be satisfied doubles. There are not enough variables to satisfy all of them, and spectral pollution appears. Edge elements [5], another numerical approach based on triangles, are known to give results without spectrum pollution. However, it is expected that the precision needed in MHD cannot be achieved.

After presenting Maxwell's equations for a bounded, unmagnetized plasma in a cylindrical waveguide of radius $r=1$, the COOL method is briefly presented. Specifically, a new type of basis functions is presented. They are zero in most of the Gauss points used for the numerical integration, thus reducing the number of operations to compute the matrix elements. To show the efficiency of the COOL method, a cylindrical infinitely long plasma configuration is considered. With a Fourier analysis in the angular and longitudinal directions, the homogeneous plasma wave spectrum is analytically tractable. Numerically, this 1D geometry is considered as a 2D geometry, the angular variation is numerically resolved. In fact, numerical difficulties appearing in a toroidal geometry relevant to ITER (www.iter.org) computations also appear in a cylinder: The periodicity in the longitudinal direction simulates the toroidal periodicity, and the angular direction behaves like the poloidal angle in a torus. A variable transformation done to satisfy the

conditions at the magnetical axis leads to a weak form with radial coefficients giving rise to new numerical challenges.

Results obtained with the COOL method are compared with analytically computed spectra and waveforms for homogeneous and non-homogeneous plasmas.

2 Maxwell's equations

2.1 The eigenvalue problem

A plasma filled waveguide can be represented by the **curl**(**curl**) eigenvalue problem

$$\nabla\times\nabla\times\vec{E}=\frac{1}{c^2}(\omega^2-\omega_p^2)\vec{E}, \quad \text{in } \breve{\Omega}, \tag{2.1}$$

$$\vec{E}\times\vec{n}=0, \quad \text{on } \Gamma_D, \tag{2.2}$$

$$\vec{E}(r,\theta,0)=\vec{E}(r,\theta,L), \quad \text{on } \Omega, \tag{2.3}$$

$$e_r(0,\theta,z)=0, \quad \text{on } \Gamma_0, \tag{2.4}$$

$$e_\theta(0,\theta,z)=0, \quad \text{on } \Gamma_0, \tag{2.5}$$

$$E_z(0,\theta,z)=E_z(0,0,z), \quad \text{on } \Gamma_0, \tag{2.6}$$

where $\breve{\Omega}$ is the cylinder domain obtained by rotating the rectangle $\{(r,z)\in]0,1[\times]0,L[\}$ around the axis $\Gamma_0=\{(r=0,z)$ with $z\in]0,L[\}$. In (2.1) $\omega_p(r)$ is the common electron plasma frequency and c is the velocity of light, while in (2.2) $\vec{n}$ denotes the outer unit normal along the boundary

$$\Gamma_D=\{(r=1,\theta,z)\,(\theta,z)\in]0,2\pi[\times]0,L[\}.$$

The periodicity condition in (2.3) is written on

$$\Omega=\{(r,\theta),r\in]0,1[\text{ and } \theta\in[0,2\pi[\}$$

and of this making, the eigenvalue problem (2.1)-(2.6) is replaced by a collection of bidimensional problems in which the non-zero complex function

$$\vec{E}(r,\theta,z)=\vec{E}(r,\theta)e^{ikz}\equiv\left(\frac{1}{r}e_r,\frac{1}{r}e_\theta,ie_z\right)e^{ikz},$$

and k is the longitudinal wave number.

We introduce the space of admissible functions

$$V(\text{curl}):=\{\vec{e}\,|\,\vec{e}\in H_1(\text{curl};\Omega), \quad \vec{e}\times\vec{n}=0\,\text{on}\,\partial\Omega\},$$

where (see [7])

$$H_1(\text{curl};\Omega):=\left\{\vec{e}|\,\vec{e}\in\left(L_1^2(\Omega)\right)^3, \quad \text{curl}\vec{e}\in L_1^2(\Omega)\right\}$$

and $L_1^2(\Omega)$ is the space of measurable functions ψ such that

$$||\psi||_{L_1^2(\Omega)} = \left(\int_\Omega \psi(r,\theta)\,\psi^*(r,\theta)\,\mathrm{rdrd}\theta \right)^{\frac{1}{2}} < \infty,$$

where * stands for complex conjugate. $||\vec{e}||^2_{L_1^2(\Omega)}$ is a norm induced by the inner product $(\vec{e},\vec{f}^*)_1$ of the complex fields $\vec{e}$ and $\vec{f}$

$$\left(\vec{e},\vec{f}^*\right)_1 := \int_\Omega \vec{e}(r,\theta)\cdot\vec{f}^*(r,\theta)\,\mathrm{rdrd}\theta, \quad \text{and} \quad ||\vec{f}||^2_{L_1^2(\Omega)} := \left(\vec{f},\vec{f}^*\right)_1.$$

One obtains the variational formulation of the problem by taking the inner product of (2.1) with any $\vec{f} \in V(\mathrm{curl})$. After integration by parts the problem becomes: Find $\vec{e} \in V(\mathrm{curl})$ and $\omega^2 \in \mathbb{R}^+$ such that

$$\mathcal{A}\left(\vec{e},\vec{f}^*\right) := \left(\vec{\nabla}\times\vec{e},\vec{\nabla}\times\vec{f}^*\right)_1 + \mathcal{L}\left(\frac{\omega_p^2}{c^2},\vec{e},\vec{f}^*\right) = \mathcal{L}\left(\frac{\omega^2}{c^2},\vec{e},\vec{f}^*\right), \forall\,\vec{f} \in V(\mathrm{curl}). \tag{2.7}$$

where

$$\mathcal{L}\left(s,\vec{e},\vec{f}^*\right) = \left(\frac{s}{r^2}e_r,f_r^*\right)_1 + \left(\frac{s}{r^2}e_\theta,f_\theta^*\right)_1 + (se_z,f_z^*)_1.$$

In (2.7) the expression of the curl is given by

$$\vec{\nabla\times}e = \left[\frac{i}{r}\left(\frac{\partial e_z}{\partial\theta} - ke_\theta\right), i\left(\frac{k}{r}e_r - \frac{\partial e_z}{\partial r}\right), \frac{1}{r}\left(\frac{\partial e_\theta}{\partial r} - \frac{1}{r}\frac{\partial e_r}{\partial\theta}\right)\right], \tag{2.8}$$

and $\vec{e} = (e_r,e_\theta,e_z)$. We remind that

$$e_r(r,\theta) = rE_r(r,\theta), \quad e_\theta(r,\theta) = rE_\theta(r,\theta), \quad e_z(r,\theta) = -iE_z(r,\theta).$$

3 The COOL method

3.1 Formulation in the reference element

To introduce the COOL (Constraint Oriented Library) method [2], let us start the presentation on the reference domain $\Omega = \Lambda^2$ with $\Lambda := (-1,+1)$. Let $\Sigma_{GL} = \{(\zeta_i,\omega_i); 1 \le i \le p\}$ denote the sets of Gauss-Legendre nodes and weights associated to polynomials of degree p. These quantities are such that :

$$\forall\,\Phi \in \mathbb{P}_{2p-1}(\Lambda), \qquad \int_{-1}^{+1} \Phi(\zeta)\,d\zeta = \sum_{j=1}^{p} \Phi(\zeta_j)\,\omega_j, \tag{3.1}$$

where $\mathbb{P}_p(\Lambda)$ denotes the space of polynomials with degree $\le p$. We recall that the nodes $\zeta_i (1 \le i \le p)$ are solution to $L_p(\xi) = 0$ where L_p is the Legendre polynomial of degree p

(see [6]). For our purpose, let us introduce two polynomial basis functions defined in the reference domain:

$$h_j(x) = -\beta_j \frac{(1-x^2)L_p(x)}{(x-x_j)(x-\zeta_1)}, \qquad 0 \le j \le p, \tag{3.2}$$

$$g_j(x) = h_j(x) - \beta_j L_p(x) = \beta_j \frac{(x(x_j+\zeta_1) - x_j\zeta_1 - 1)L_p(x)}{(x-x_j)(x-\zeta_1)}, \tag{3.3}$$

where β_j normalizes $h_j(x_j)=1$ and the nodes $(x_j)_{(0\le j\le p)}$ are such that $x_0=-1$, $x_p=+1$ and $x_i=\zeta_{i+1}, i=1,\cdots,p-1$. The functions $h_j(x)$ are polynomials of degree p, continuous across element borders. They are used to represent derivatives that are polynomials of degree $p-1$, discontinuous across element borders. They verify $h_i(x_j)=\delta_{ij}$, where δ_{ij} is Kronecker's delta symbol. The functions $g_j(x)$ are polynomials of degree $p-1$, discontinuous across element borders, and are used to represent variations in directions without derivatives. The set of $(p+1)$ functions $g_i(x) \in \mathbb{P}_{p-1}(\Lambda)$ is linearly dependent. However, any combination of p elements in the list is linearly independent. We therefore arbitrarily discard one element in the set $\{g_i(x)\}_{i=0}^{p}$ (for, instance the first one, $g_0(x)$) and use the remaining elements to span the $\mathbb{P}_{p-1}(\Lambda)$ space dependence of the two-dimensional spectral element.

We therefore build a set of convenient auxiliary functions:

$$e_{xp}(r,\theta) = \sum_{k=0}^{p}\sum_{\ell=0}^{p} \overline{e}^{x}_{k\ell} h_k(r) h_\ell(\theta), \qquad e_{xp} \in \mathbb{P}_p(\Lambda)\otimes\mathbb{P}_p(\Lambda), \tag{3.4}$$

$$e^{(0)}_{xp}(r,\theta) = \sum_{k=1}^{p}\sum_{\ell=1}^{p} \overline{e}^{x}_{k\ell} g_k(r) g_\ell(\theta), \qquad e^{(0)}_{xp} \in \mathbb{P}_{p-1}(\Lambda)\otimes\mathbb{P}_{p-1}(\Lambda), \tag{3.5}$$

$$e^{(1)}_{xp}(r,\theta) = \sum_{k=0}^{p}\sum_{\ell=1}^{p} \overline{e}^{x}_{k\ell} h_k(r) g_\ell(\theta), \qquad e^{(1)}_{xp} \in \mathbb{P}_{p}(\Lambda)\otimes\mathbb{P}_{p-1}(\Lambda), \tag{3.6}$$

$$e^{(2)}_{xp}(r,\theta) = \sum_{k=1}^{p}\sum_{\ell=0}^{p} \overline{e}^{x}_{k\ell} g_k(r) h_\ell(\theta), \qquad e^{(2)}_{xp} \in \mathbb{P}_{p-1}(\Lambda)\otimes\mathbb{P}_{p}(\Lambda). \tag{3.7}$$

The number of variables has first been extended from 3 $(e_{rp}, e_{\theta p}, e_{zp})$ to 12 $\left(e_{xp}, e^{(0)}_{xp}, e^{(1)}_{xp}, e^{(2)}_{xp}\right)$ (here and until the end, the index x denotes r, θ or z), then restricted again to 3 by imposing the 9 moment integral conditions

$$\int_\Omega \left[e_{xp}(r,\theta) - e^{(i)}_{xp}(r,\theta)\right] \eta(r,\theta)\, r\,dr\,d\theta = 0. \tag{3.8}$$

In the test functions

$$\eta(r,\theta) = r^j \theta^\ell, \tag{3.9}$$

$0 \le j,\ell \le p-1$ for $i=0$, $0 \le j \le p$ and $0 \le \ell \le p-1$, for $i=1$, and $0 \le j \le p-1$ and $0 \le \ell \le p$ for $i=2$. The goal is now to represent the new variables such that each term in Eq. (2.8)

has the same functional dependence and the same regularities across element borders. One can easily prove that due to the nature of the boundary conditions (2.2) and (2.4)-(2.6) the expansions (3.5)-(3.7) involve the *same* sets of parameters $\{\bar{e}^x_{k\ell}\}$, that are equal to the values of $e_{xp}(\zeta_i,\zeta_j)$. Note that if using an integration scheme with p Gauss points, the moment equations (3.8) are satisfied. The only difference between $e_{xp}(x,y)$,$e^{(0)}_{xp}(x,y)$, $e^{(1)}_{xp}(x,y)$ and $e^{(2)}_{xp}(x,y)$ lies in the degree of the basis functions. Let us now introduce the expansions (3.5)-(3.7) into the variational formulation (2.7). The new problem reads: Find $\vec{e}\in V(\text{curl})\cap\mathbb{P}_p(\Omega)^3$ and $\omega^2\in\mathbb{R}^+$ such that $\forall\,\vec{f}\in V(\text{curl})\cap\mathbb{P}_p(\Omega)^3$

$$\mathcal{A}\left(\vec{e},\vec{f^*}\right):=\left(\vec{\nabla}\times\vec{e},\vec{\nabla}\times\vec{f^*}\right)_p+\mathcal{L}_p\left(\frac{\omega_p^2}{c^2},\vec{e},\vec{f^*}\right)=\frac{\omega^2}{c^2}\mathcal{L}_p\left(1,\vec{e},\vec{f^*}\right), \tag{3.10}$$

where

$$\mathcal{L}_p\left(s,\vec{e},\vec{f^*}\right)=\left(\frac{s}{r^2}e_r^{(0)},f_r^{(0)*}\right)_p+\left(\frac{s}{r^2}e_\theta^{(0)},f_\theta^{(0)*}\right)_p+\left(se_z^{(0)},f_z^{(0)*}\right)_p$$

and $s(r,\theta)$ denotes a scalar function varying in space. The notation $(\cdot,\cdot)_p$ stands for the Gauss-Legendre numerical integration. In (3.10) the expression of the curl is now

$$\vec{\nabla\times}e=\left[\frac{i}{r}\left(\frac{\partial e_z^{(2)}}{\partial\theta}-ke_\theta^{(0)}\right),i\left(\frac{k}{r}e_r^{(0)}-\frac{\partial e_z^{(1)}}{\partial r}\right),\frac{1}{r}\left(\frac{\partial e_\theta^{(1)}}{\partial r}-\frac{1}{r}\frac{\partial e_r^{(2)}}{\partial\theta}\right)\right]. \tag{3.11}$$

3.2 The multi-element Case

The transition to the multi-element approximation is straightforward. We partition $\breve{\Omega}$ into N^2 square subdomains Ω_e of equal size $h=2/N$, and

$$\breve{\Omega}=\cup_{e=1}^{N^2}\Omega_e.$$

The problem (3.10) now writes :

$$\mathcal{A}_h\left(\vec{e}_h,\vec{f}_h^*\right)=\frac{\omega^2}{c^2}\mathcal{L}_h\left(1,\vec{e}_h,\vec{f}_h^*\right), \tag{3.12}$$

with

$$\mathcal{A}_h\left(\vec{e},\vec{f^*}\right)=\sum_{e=1}^{N^2}\left(\vec{\nabla}\times\vec{e},\vec{\nabla}\times\vec{f^*}\right)_h^e+\mathcal{L}_h\left(\frac{\omega_p^2}{c^2},\vec{e}_h,\vec{f}_h^*\right), \tag{3.13}$$

$$\mathcal{L}_h\left(s,\vec{e}_h,\vec{f}_h^*\right)=\sum_{e=1}^{N^2}\left[\left(\frac{s}{r^2}e_r^{(0)},f_r^{(0)*}\right)_h^e+\left(\frac{s}{r^2}e_\theta^{(0)},f_\theta^{(0)*}\right)_h^e+\left(se_z^{(0)},f_z^{(0)*}\right)_h^e\right].$$

The notation $(\cdot,\cdot)_h^e$ stands for any numerical integration that computes the integral on Ω_e exactly, and each subdomain Ω_e must be mapped onto the reference domain. Note that we choose the same local variables in all expansions. As a consequence, we can choose the same mesh as in the case of standard hp methods.

Table 1: Comparison between analytic and numerical results with COOL of the first 21 discrete eigenvalues of the waveguide spectrum with $\omega_p^2=0$. The poloidal and radial wave numbers are m, and s, respectively.

discrete mode number	*type*	m	s	*analytic*	*COOL N=2, p=12*	*degeneracy*
				0	0	553
1/2	TE	±1	1	4.38994	4.389957717	2
3	TM	0	1	6.7831859630	6.783185963	1
4/5	TE	±2	1	10.3284	10.328363214	2
6	TE	0	2	15.681970642	15.681970642	1
7/8	TM	±1	1	15.6820	15.681970642	2
9/10	TE	±3	1	18.6500	18.6499885	2
11/12	TM	±2	1	27.3746	27.374616427	2
13/14	TE	±4	1	29.2763	29.2764	2
15/16	TE	±1	2	29.4243	29.424282047	2
17	TM	0	2	31.471262344	31.471262343	1
18/19	TM	±3	1	41.7064	41.706466	2
20/21	TE	±5	1	42.1602	42.16	2

4 Numerical results and discussion

4.1 The homogeneous plasma

First we start this section with the homogeneous plasma for which ω_p is constant in the plasma. This is the test case having classical analytical solutions by means of which we validate the numerical approach. In fact, the **curl**(**curl**) eigenvalue problem (2.1)-(2.6) has three classes of eigensolutions. One is given by

$$\omega^2=\omega_p^2, \quad \nabla\vec{\times}E=0. \tag{4.1}$$

When ω_p is constant, an infinitely degenerate solution $\omega^2=\omega_p^2$ is found. Moreover, the equations (2.1) reduce to the Bessel equation

$$r^2\mathcal{Z}''+r\mathcal{Z}'+\left(\kappa^2r^2-m^2\right)\mathcal{Z}=0, \tag{4.2}$$

where $\kappa^2=\frac{1}{c^2}(\omega^2-\omega_p^2)-k^2$. The mode number m is due to the Fourier expansion $E_z(r,\theta)=E_z(r)e^{im\theta}$ and the solution is $\mathcal{Z}(r)=J_m(\kappa r)$. Two discrete classes of eigensolutions can be obtained by imposing the boundary conditions $\mathcal{Z}(r=1)=0$ and $\mathcal{Z}'(r=1)=0$. The first condition leads to the Transverse Magnetic (TM) modes, and the second condition to the Transverse Electric (TE) modes. Their waveguide frequency spectra are given by

$$\omega^2=\omega_p^2+c^2\left(j_{m,s}^2+k^2\right), \quad s=1,2,3,\cdots \quad \text{(TM)}, \tag{4.3}$$

$$\omega^2=\omega_p^2+c^2\left(j_{m,s}'^2+k^2\right), \quad s=1,2,3,\cdots \quad \text{(TE)}, \tag{4.4}$$

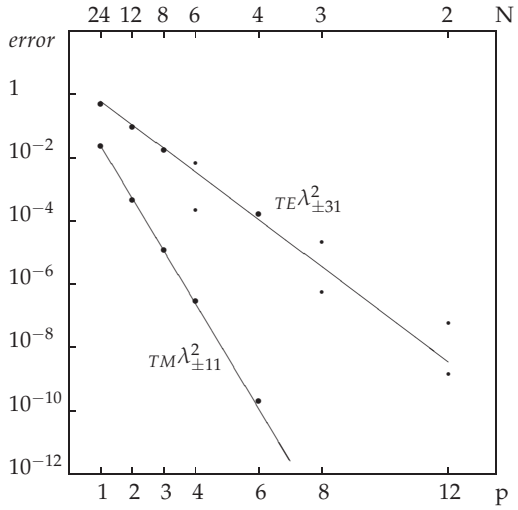

Figure 1: COOL method: Exponential convergence of the ($\pm$ 1, 1) TM mode ($\lambda^2_{=}$15.681970642, lower thick points), and of the ($\pm$ 3, 1) TE mode ($\lambda^2 = 18.64998852$, upper thick an fine points) as a function of the polynomial degree p, fixing Np=24.

where $j_{m,s}$ and $j'_{m,s}$ are the zeros of the Bessel function $J_m(\kappa r)$ and its derivative $J'_m(\kappa r)$, respectively. If the plasma is absent, ω_p^2=0, and the usual waveguide modes are obtained from these expressions. This case is discussed in the result Section 4.2.

4.2 Eigenmodes of an empty cylindrical waveguide

The COOL method [2] is applied to the variational form, Eq. (3.12), with $\omega_p^2 = 0$ in the empty waveguide. In this case, the Langmuir oscillations are reduced to pure electrostatic solutions at $\omega^2 = 0$. This is a correct result also contained in the Maxwell equations in vacuo: Electrostatics! When choosing N elements in both directions and a polynomial degree of p, the infinite degeneracy of the eigenvalue ω^2=0 is represented numerically by $Np(Np-1)+1$ eigenvalues with ω^2=0. The discrete eigenvalues are computed choosing N=2 and p=12. There are only physically relevant eigensolutions with the exact degeneracy, and the precision of the eigenvalues is perfect. All the discrete eigenvalues converge as in the traditional spectral method. In Table 1 we present a comparison between analytic and numerical results with COOL. The first 21 discrete eigenvalues of the waveguide spectrum with ω_p^2=0 are listed. The poloidal wave number is m, the radial wave number s. The degeneracy of the irrotational eigenmodes at ω^2=0 is $Np(Np-1)+1$=553. The analytic values of the waveguide modes, Eqs. (4.3) and (4.4), are computed with the Bessel function zeroes taken from Abramowitz-Stegun [1]. These are impressive results since to achieve $\vec{\nabla} \times \vec{E} \equiv 0$ implies that this numerical method is able to put all three vector components in Eq. (2.8) identically to zero everywhere and this inspite of the $1/r$ coefficients in the different terms.

In Fig. 1 is shown the exponential convergence of the ($\pm$ 1, 1) TM mode ($\lambda^2_{\pm 11} =$ 15.681970642, lower thick points), and of the ($\pm$ 3, 1) TE mode ($\lambda^2_{\pm 31} =$18.64998852, upper thick an fine points), fixing $Np=24$, for instance, if $p=8$, $N=3$. One clearly recognizes exponential convergence as a function of p.

4.3 The continuous spectrum

If ω_p varies in space, a continuous spectrum

$$\min_{\vec{r}} \omega_p^2(\vec{r}) \leq \omega^2 \leq \max_{\vec{r}} \omega_p^2(\vec{r}) \tag{4.5}$$

appears. In addition, a "discrete mode" can lie in the continuous spectrum, the continuous and the discrete eigensolutions couple, and the resulting eigensolutions are not further curl-free. This corresponds to the physically relevant Alfvén wave heating mechanism in fusion research [3]. In fact, the energy of a global eigenmode can be deposited on an internal surface on which the frequency of the continuous mode corresponds to the frequency of the "global eigenmode". The degenerate continuum modes are difficult to capture numerically.

A simple choice of a radially varying function is $\omega_p^2 = 1-r^2$ (see Fig. 2). The continuous spectrum is then represented by an infinite number of eigensolutions. For any value in the frequency band $0 \leq \omega_p^2(r) \leq 1$ there is a singular eigenmode which, in the mathematical sense, is not a function but a distribution. Only weighted integrals of such eigensolutions over finite frequency bands make physical sense. Numerically, $Np(Np-1)+1$ eigenvalues with singular eigenmodes are found between 0 and 1; this number corresponds to that of degenerate eigenvalues given in Table 1.

The simply structured $m=0$ modes show the required $\pm 1/(r-r_s)$ behaviour on the E_r component. The width of the peak is proportional to the mesh size, i.e., $\sim 1/N$, and its height $\sim \sqrt{N}$ such that the norm

$$\int_0^1 E_r^2 r dr \approx \text{const};$$

see Fig. 3, where results for the lowest order COOL method ($p=1$) are shown. The computed eigenmodes are, however, different from what had been found in MHD [9]. Without applying the COOL method to the corresponding initial value and/or linear response problems (resonant absorption of electromagnetic waves) it is difficult to know whether these discrete eigenfunctions can well represent the distributions associated with the continuous spectrum. This is left for future investigations.

The eigenfunctions show the right dependence on the frequency, see Fig. 4. Using higher order COOL methods leads to a delocalization of the continuum modes (see Fig. 5). This has been produced with $p=8$ and 4 radial elements. Whether this Gibbs phenomenon makes the method ill-suited for calculations in the continuum is *a-priori* not clear, but it could well be that an optimum between N and p must be sought in this case.

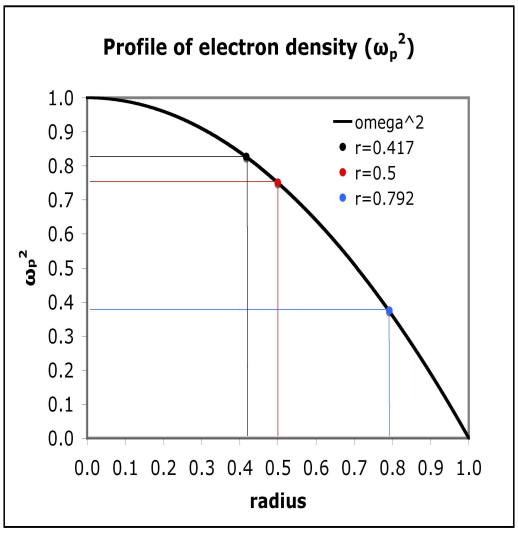

Figure 2: The parabolic density profile $\omega_p^2(r)$ leading to the continuous frequency spectrum in the range $0<\omega^2<1$. The three points are the numerical result (eigenfrequency and localization) taken from the modes shown in Fig. 4.

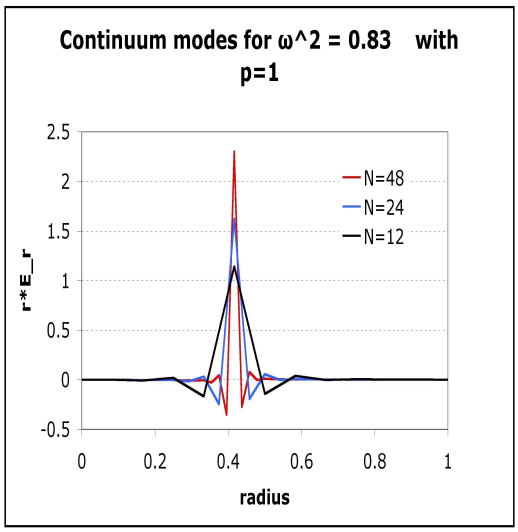

Figure 3: Radial structure of the numerically computed, now discrete, eigenmodes in the continuum for $k=1$, $m=0$. Three different resolutions are shown. The modes are localized at $r=0.417$ and have $\omega^2=0.8284$, 0.8273 and 0.8268 for $N=12$, 24 and 48.

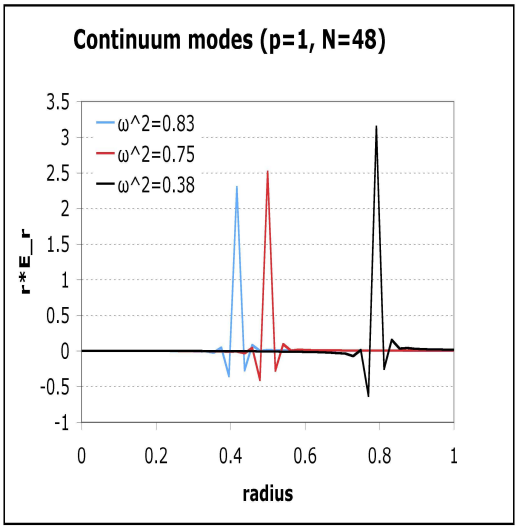

Figure 4: Three different continuum modes with the same method and resolution. Their frequency precisely corresponds to their localization, see Fig. 2.

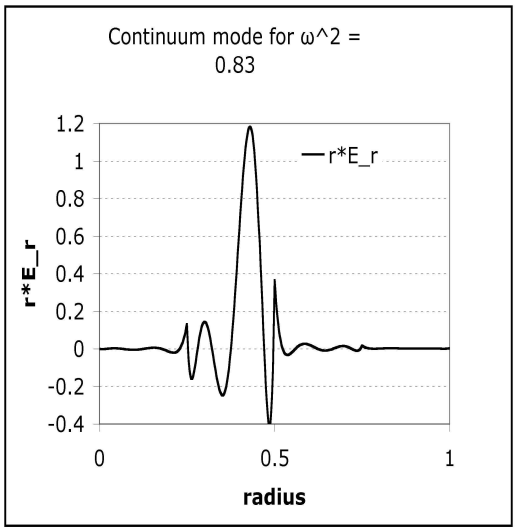

Figure 5: Continuum eigenmode in a high-p COOL method. Its distribution character has yet to be studied.

Definite answers can only be given by a linear response calculation where the singular solutions appear under an integral, leading to a regular function.

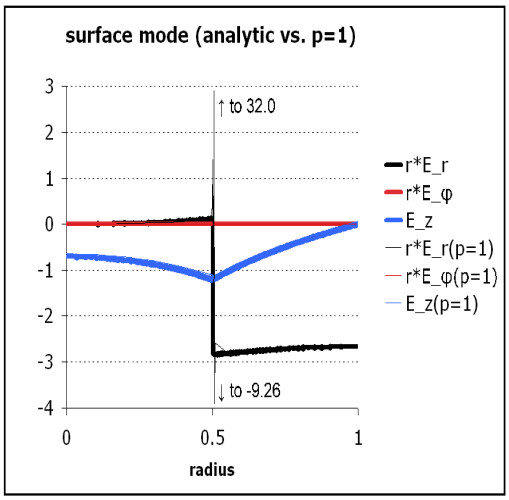

Figure 6: An $m=0$ continuum mode which contains the surface mode information. There are several such modes (distributions!) with neighboring frequencies. The one shown has $\omega=0.57$ whereas the analytical value is $\omega=0.6012$. In a certain distance from the plasma surface the global part of the distribution coincides well with the analytical surface mode as it should.

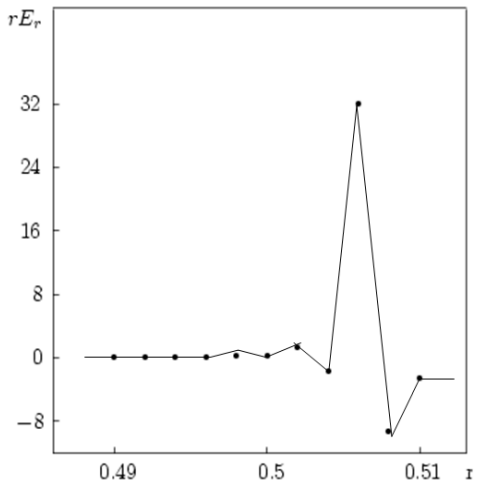

Figure 7: Enlarged representation of the rE_r component of the eigenmode represented in Fig. 6.

4.4 Waveguide partially filled with uniform plasma

The case with a stepwise uniform plasma frequency is analytically accessible. We do not discuss these calculations here. We just show numerical results and try to explain them. The plasma we consider here, is a uniform one with $\omega_p=3$ in the inner half ($r\leq 0.5$) of the waveguide. The space between the plasma and the metallic shell ($0.5<r<1$) is empty, $\omega_p=0$. In such a situation, there is always for each m a so-called surface mode with a frequency between 0 and ω_p. In the present case, its frequency is 0.6 for $m=0$. A jump in ω_p cannot be treated numerically as such. We have to let the profile jump gradually varying in a small radial region. The step is represented by a steep slope with a width of 0.02 and three domains are used for the discretization: $0\leq r\leq 0.49$ with $\omega_p=3$, $0.49\leq r\leq 0.51$ with $\omega_p=76.5-150r$, and $0.51\leq r\leq 1$ with $\omega_p=0$. In Fig. 6, are represented the three analytically computed components of the eigensolution with the jump in ω_p at $r=0.5$. Superimposed is the numerical solution with the steep gradient in ω_p instead of the jump, $N_r=10$ in all the three radial domains, $N_\theta=2$ in azimuthal direction, and $p=1$ in both directions. The two solutions are normalized such that the values of rE_r are equal at $r=1$. The analytic solution has $\omega^2=0.361$ and the numerical one $\omega^2=0.330$. Their eigenfunctions agree well apart from the area $0.49\leq r\leq 0.51$, where the numerical problem possesses a discretized continuum with its corresponding singularities. To let details of the numerical eigenmode appear, we enlarge the domain around $r=0.5$ (see Fig. 7). Whereas the analytical behaviour of the rE_r component develops a jump, the nu-

merically computed rE_r component shows the typical behaviour of a continuous mode. The maximum is at $r=0.506$ corresponding to $\omega_p^2=0.36$. This is a very satisfying result. This effect is even more pronounced when higher p and lower N_r are used.

5 Conclusions

It has been shown that the COOL method is able to reproduce exactly the infinite degeneracy of the irrotational Langmuir oscillations in a homogeneous plasma. This is an important result since the geometry was not Cartesian and two of the three variables were transformed to be able to impose the regularity conditions at the axis. This shows that the COOL method is able to satisfy the physical internal constraint $\nabla\times\vec{E}=0$ precisely, even with radially varying coefficients in the variational form. This shows that the COOL method satisfies the constraints in collocation manner, i.e. at all the Gauss points.

Besides the correct reproduction of an infinite degeneracy, it is possible to compute the continuous spectrum with high precision. The number of eigenvalues in the continuous region augments with $Np(Np-1)+1$. Instead of the eigenfunctions of the distributional type demanded by the theory, the numerical approximation leads, at least for first-order polynomials, to highly localized modes with properties in agreement with earlier methods of discretization. The higher-order approximations lead to less localized modes whose distributional character can only be investigated in an application to a linear response problem. In this context an encouraging result is the well-represented surface mode which has been found in this paper.

Cavity modes have been obtained with only few elements to great precision even in cases with abrupt changes of mesh size and medium (coefficients of differential equation). Despite the high-order polynomial approximations, the only slight Gibbs phenomena observed at the place of these changes seem not to affect the numerical eigenmodes.

Acknowledgments

The authors would like to thank the reviewers for the remarks that strongly improved the manuscript.

References

[1] M. Abramowitz and I.A. Stegun, Handbook of Mathematical Functions, Dover Publications, New York, 1970.

[2] E. Ahusborde, R. Gruber, M. Azaiez and M.L. Sawley, Physics-conforming constraints-oriented numerical method, Phys. Rev. E, 75, 056704 (2007).

[3] Appert K., Balet B., Gruber R., Troyon F. and Vaclavik J.,"Optimization of resonant absorption of Alfvén waves in low-Beta plasmas", in Plasma Physics and Controlled Nuclear Fusion Research 1980 (Proc. 8th Int. Conf. Brussels,1980), Vol.2, IAEA, Vienna (1981) 43 and references therein.

[4] M. Azaiez, M. Deville, R. Gruber and E. Mund, A new *hp* method for the -grad(div) operator in non-Cartesian coordinates, accepted for publication in Applied Numerical Mathematics (2007).
[5] A. Bossavit, Computational Electromagnetism, Academic Press, 1998.
[6] M.O. Deville, P.F. Fischer and E.H. Mund,High-Order Methods for Incompressible Fluid Flow, Cambridge University Press, Cambridge, 2002.
[7] Girault V. and Raviart P., Finite Element Methods for Navier-Stokes Equations, Series in Computational Mathematics, Springer-Verlag, Berlin, 1986.
[8] R. Gruber, Finite hybrid elements to compute the ideal MHD spectrum of an axisymmetric plasma, J. Comp. Phys., 29 (1978), 379-389.
[9] R. Gruber and J. Rappaz, Finite Element Methods in Linear Ideal MHD, Springer Series in Computational Physics, (Springer-Verlag, Berlin, 1985).
[10] F. Troyon, R. Gruber, H. Saurenmann, S. Semenzato and S. Succi, MHD limits to plasma confinement, Plasma Phys., 26 (1983), 209-215.